Bulletin of Pure and Applied Sciences
Geology, Vol.44F, No.2,
July-December 2025: P.107-123
Original Research Article

Print version ISSN 0970 4639
Online version ISSN 2320 3234
Available online at www.bpasjournals.com

Petrogenesis of Fractionated High Ba–Sr Granitoids from the Southern Kyrdem Pluton, Northeast India: Evidence for complex Mantle–Crust Interaction

***Liza Gogoi[1], Sorokhaibam Kavita Devi[1], and G. Lamzamuan[1]**

Author's Affiliations:
[1]Department of Geology, Mizoram University, Aizawl, Mizoram, India

***Corresponding Author:** Liza Gogoi, Department of Geology, Mizoram University, Aizawl, Mizoram, India
E-mail: lizagogoi67@gmail.com

Received on 27.09.2025, Revised on 19.11.2025, Accepted on 25.11.2025

How to cite this article: Gogoi L., Devi S.K., and Lamzamuan G. (2025). Petrogenesis of Fractionated High Ba–Sr Granitoids from the Southern Kyrdem Pluton, Northeast India: Evidence for complex Mantle–Crust Interaction. *Bulletin of Pure and Applied Sciences- Geology,* 44F (2), 107-123.

Abstract:
The high Ba–Sr granites as indicators of crust–mantle interaction processes is becoming more widely acknowledged. These uncommon melts typically originated from hydrous mafic sources in the lower crust or from partial melting of basaltic underplates. The present investigation focuses on Late Cambrian southern Kyrdem Granitoid (KG) in the Shillong Plateau, India, using field, petrographic and geochemical studies to depict its tectonics, magmatic processes, and genesis of one such uncommon rock suite. The KG has porphyritic and non-porphyritic varieties, with patches of nepheline syenites, suggesting magma mixing, hybridization, and multiple intrusive episodes. Hydrothermal inputs are indicated through petrographic investigations showing different intergrowths textures. Whole-rock geochemical studies suggest that granitoids are alkalic to alkalic-calcic and metaluminous in nature. With high concentrations of Ba (709-3000 ppm) and Sr (103-586 ppm), moderate Rb (~295 ppm), low Y, U (1.9–4.7 ppm), and negative Eu anomalies, the KG are comparable to other high Ba-Sr granites. Such enrichment of Ba, Sr is likely controlled by feldspar, micas and accessory mineral phases. This elevated concentration suggesting a highly evolved, fractionated magma, potentially with subduction-modified mantle contributions, akin to sanukitoid-type granites. The low Ba/Th (avg.~58.5), U/Th (~0.15), along with the low Mg# values (~18.7) and La/Sm ratios, suggest that these melts may originated from an enriched lithospheric mantle that had been metasomatized by subducted sediment-derived melts with a minimal crustal input. The tectonic diagram infers emplacement during a late-collisional to post-collisional stage. Thus the findings improved our understanding of multiple genesis of high Ba-Sr granitoid systems.

Keywords: *Kyrdem Granitoids, High Ba–Sr Granites, Petrogenesis, Pan-African Orogeny, Shillong Plateau.*

INTRODUCTION

Over geological time, granitoids have been intruded both spatially and temporally, allowing us to comprehend how the Earth's composition and evolution style have changed over time and space. Granitoids can be found forming in almost all tectonic environments, such as subduction zones, rift zones (continental and oceanic islands), hot spots, mountain belts, and even mid-

ocean ridges, which provide insights into the intricate crust-mantle dynamics (Rudnick and Gao 2003). As a result, geoscientists have been fascinated by the genesis of these coexisting unusual granitoids and by understanding the tectonic environments that surround them. An example of such, high Ba-Sr granitoids with high Zr are rare species because they need exceptionally high temperatures and lower crust melting, where plagioclase is repressed and zircon approaches saturation conditions uncommon in typical granite formation (Fowler et al., 2001; Zhang et al., 2021). These rocks are quite rare and geodynamically unique granite types since such melts usually only occur during extraordinary crust–mantle interaction events like delamination or slab break-off. The Kyrdem pluton on the Shillong Plateau in northeastern India is home to one such noteworthy example of complex granitoids. The Shillong Plateau, which is an important Archaean gneissic complex of the Indian craton, was subjected to a major continental crust buildup during the early Paleozoic period (535–430 Ma: Kumar et al. 2017). The rise of huge granitoid plutons (South Khasi, Mylliem, Nongpoh, and Kyrdem) characterized this period (Fig.1). The tectonic regime seems to be greatly dependent on pre-existing rifts and structural lineaments, which is clearly indicated by the age sequence of the scattered plutons from the southwest to the northeast. As per Kumar et al. (2017), while the Mylliem and Kyrdem plutons are completely within the Shillong Group, the South Khasi and Nongpoh plutons rest above both the Shillong Group and the granite gneisses complex (Fig. 1). It is believed that the granitoids were laid down during the Neoproterozoic as the Pan-African orogeny migrated eastward into the eastern Gondwana block (Ghosh et al., 2005; Choudhury et al., 2012; Kumar et al., 2017). The present work aims at describing the field relationships, petrography, and geochemistry of one such granitoid (southern Kyrdem granitoids) while also discussing their petrogenetic and tectonic significance.

GEOLOGICAL SETTING

Regional geology

The Shillong (Meghalaya) Plateau is an uplifted horst-like formation that covers over 40,000 km² (Saha et al., 2010). Along with Cretaceous–Palaeogene sediments and modern alluvium, it is composed of amphibolites, a gneissic complex, basic granulites, the Shillong Group of metasediments, and a variety of intrusive units, such as granite plutons, ultramafic-alkaline-carbonatite (UKC) complexes, and the Sylhet Trap. The Shillong Plateau is a Precambrian shield with a Paleoproterozoic basement complex that has been intruded by several felsic and mafic magmatic rocks, overlain by Tertiary sediments and overlain by Shillong Group Mesoproterozoic supracrustal rocks covering the basement. The plateau is structurally bounded by notable Cenozoic faults, such as the the Dauki fault to the south, Jamuna fault to the west, and the Brahmaputra fault to the north (Hussain and Choundhury, 2023). The basement rocks include of quartzo-feldspathic gneisses, amphibolite-to-granulite-facies gneisses, migmatites, mafic granulites, and metapelitic granulites (Majumdar and Dutta, 2016; Chatterjee, 2017). The thick quartzite and phyllite layers make up the majority of the Mesoproterozoic Shillong Group. The basement group of rocks of the Shillong Plateau was intruded by three identifiable, distinct episodes of magmatic activity. The first episode was of basaltic magmatism during the Mesoproterozoic, presently represented by meta-dolerites (also termed as Khasi Greenstones), followed by an episode of granitoid plutonism (430-535 Ma) represented by Nongpoh, South Khasi, Mylliem, and Kyrdem plutons. The last episode was marked by Sylhet Trap volcanism (117 Ma) and associated UAC magmatism (Ghatak and Basu, 2013; Kumar et al. 2017; Ray et al. 2005; Yin et al. 2010). Although thicker accumulations are seen in the eastern and southwestern borders, tertiary sediments are found as peripheral deposits surrounding the plateau. The gneissic complex and the Shillong Group metasedimentary rocks are penetrated by these intrusions, which were deposited by means of pre-existing lineaments and fractures (Evans, 1964; Nandy, 1980). Pan-African orogenic processes were responsible for a major Neoproterozoic–Cambrian granitoid emplacement phase that accompanied the merging of the Eastern Gondwana supercontinent (Ghosh et al., 2005; Yin et al., 2010).

Study area

The Mylliem, Nongpoh, Kyrdem, and South Khasi felsic plutons, which were formed along major lineaments or fractures according to Mazumder's (1976, 1986), are late- to post-tectonic, diapiric intrusions result in periodic thermal events in the mantle. However, the Rb-Sr isotopic ages of the corresponding plutons (Kyrdem 479±26 Ma; Nongpoh 550±15 Ma; Mylliem 607±13 Ma; South Khasi 690±19 Ma) were established by Ghosh et al. (1991, 1994, 2005) through rock analysis. This led to the conclusion that Meghalaya experienced a protracted thermal event from 700–500 Ma of about 200 Ma period (Proterozoic-Early Palaeozoic), which was most likely connected to the Pan African–Caledonian orogeny. The Kyrdem section of the Meghalaya plateau, which was formerly known as the Kyrdem Granitoid (KG) (Fig. 1), was thought to be in the late Ordovician (479±26 Ma) period. Accordingly, the early Ordovician intrusion encompasses the Shillong Group, which transforms into an oval-shaped plutonic body with its longer axis nearly North-South aligned.

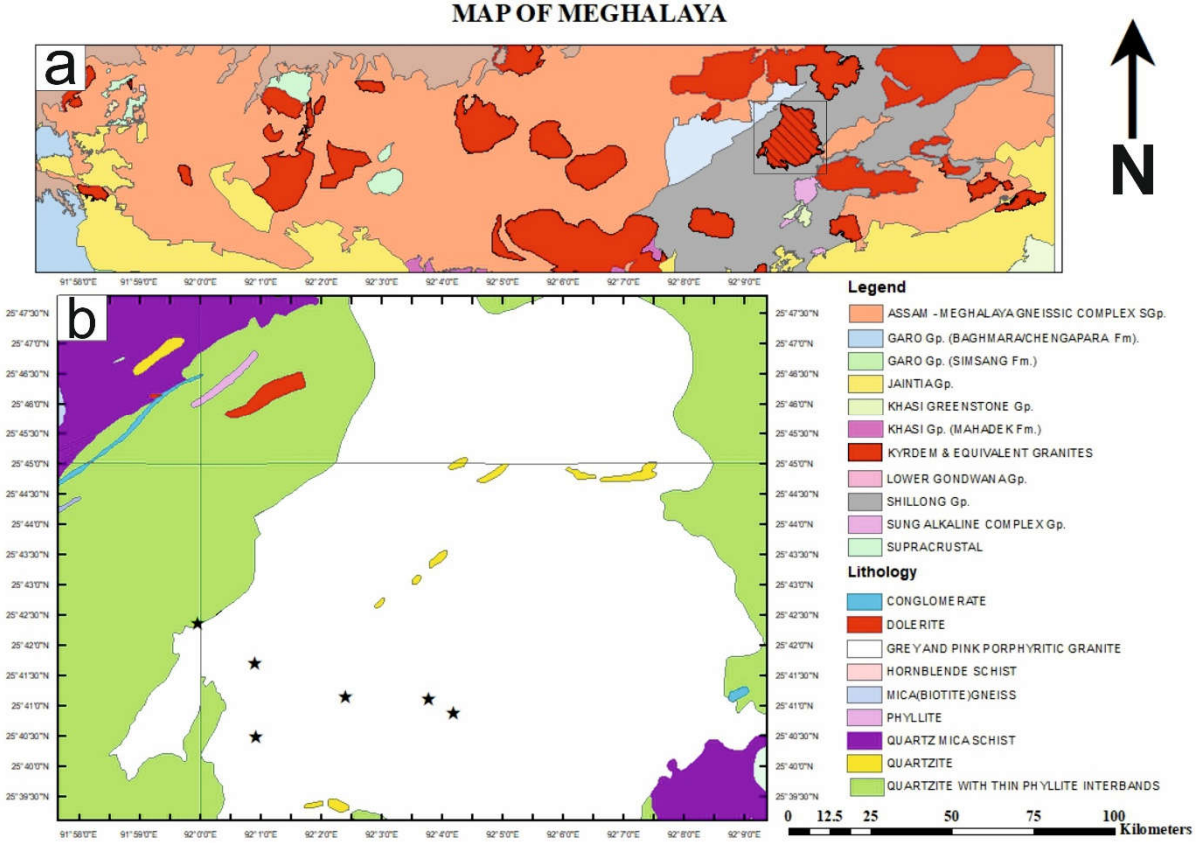

Figure 1: a) Geological Map of Meghalaya depicting different formations and all granitoid plutons (Mylliem, Nonpoh, Kyrdem and South Khasi into the Proterozoic Shillong Group of rocks and Archean basement gneisses)
b) Geological Map of Kyrdem area (modified after Hussain and Choudhury, 2023)

METHODOLOGY

In the southern part of KG pluton, systematic sampling was done away from any major lineament for petrographic and geochemical studies (Fig. 1). Leica Q-win cameras and in-built software are used for microphotography and petrographic observations. Based on the

petrographic analysis (texture, mineralogy, and alteration), six fresh, and representative in situ samples were chosen for bulk rock geochemical investigation, two from each of the coarse-grain porphyritic and non-porphyritic and fine-grain granitoids. Using a steel mortar and a corundum jaw crusher, the rock samples were further processed into *300 meshes at the CSIR-NGRI, Hyderabad, India. The pressed pellets using ED-XRF was used to analyse major oxides. To guarantee accuracy and precision, international USGS rock standards G-2 and JB-2 were used. Precision and accuracy for major aspects were found to be better than 5%. At CSIR-NGRI, India, samples trace element compositions were examined using HR-ICP-MS in accordance with Satyanarayanan et al. (2018).

RESULT AND DISCUSSION

Field Evidence

Based on field data, the southern part of KG pluton consists of coarse-grained granitoid, which are both porphyritic and non-porphyritic in nature (Fig. 2a, b), coarse to medium-grained biotite-rich granite, and medium-grained mafic granitoids (Fig. 2c) with fine-grained nepheline syenite (Fig. 2d) and several thin aplite veins (Fig. 2e). Quartz, plagioclase, biotite, and hornblende are the major minerals making up the granitoid stock. In comparison to other parts of the pluton, the size, quantity, and size of the xenolithic enclaves are high here; they can range from a few millimeters to a meter (Fig. 2f). Fine-grained fabrics KG are represented by small amounts of layered aplite veins with fine grains and recrystallised phenocrysts (plagioclase and biotite) trapped inside.

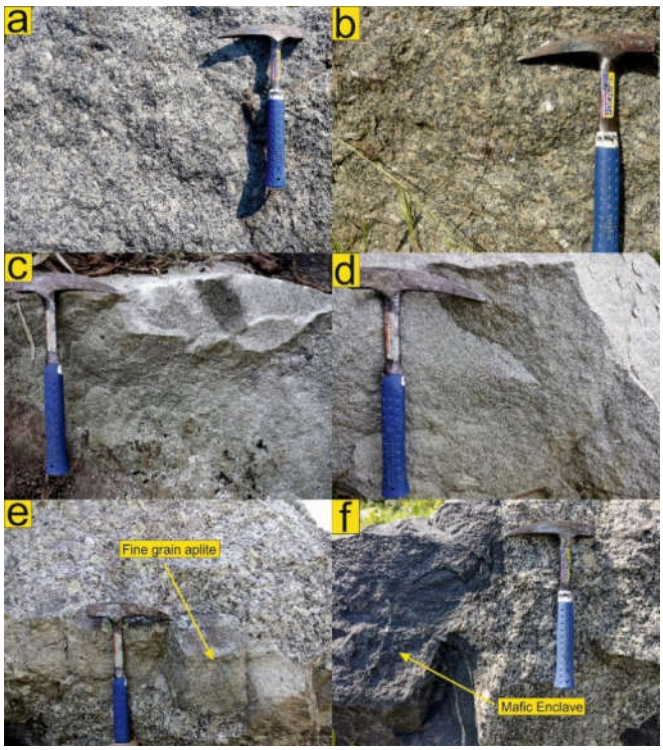

Figure 2: Field photographs of
a) Plagioclase porphyritic Kyrdem Granitoid
b) K-feldspar-rich pink coarse-grained Kyrdem Granitoid
c) Medium-grained mafic biotite-rich granitoids
d) Fine-grained Nepheline syenite
e) Fine-grained aplite flow band in medium-grained grey granite
f) Angular Micro-granular Mafic Enclave hosted in coarse-grained Kyrdem Granitoid

Petrography

The Kyrdem granitoids of the Shillong Plateau have a variety of textures and morphologies that reflect the interaction between melts, tectonic deformation and magmatic crystallisation; their leucocratic to mesocratic nature, ranging from light to intermediate compositions, illustrates the varied crystallisation and emplacement conditions; the equigranular and hypidiomorphic granular textures of the Kyrdem granitoids suggest essentially constant cooling conditions; the presence of porphyritic and fine-grained textures with K-feldspar megacrysts is another indication of magmatic and differential cooling processes. The KG pluton display a variety of rock types and textures, i.e., 1. Coarse-grained textures, both porphyritic and non-porphyritic, 2. Medium-sized grains granitoids 3. Fine-grained Nepheline syenite 4. Aplite bands etc. The majority of them are coarse-grained porphyritic granites, but there are also non-porphyritic, medium- to fine-grained rocks that show notable differences in their mineralogical and textural properties. Most porphyritic granites are composed of microcline or lath-shaped plagioclase phenocryst in a groundmass mixture of plagioclase, quartz, K-feldspar, and biotite and other accessory minerals (Fig. 3a).

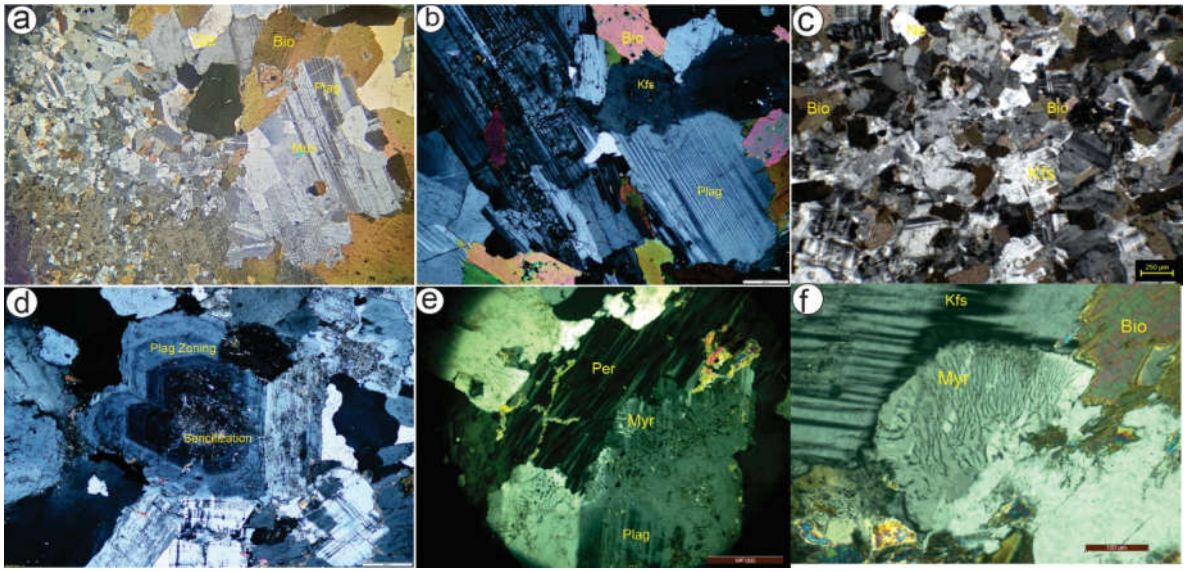

Figure 3: Microphotographs of KG showing
a) Inequigranular porphyritic texture with Phenocryst of plagioclase, quartz and biotite b) Coarse-grained KG showing assemblage of plagioclase (Plag), quartz (Qtz), and amphibole (Amp) with minor mafic minerals
c) Fine-grained Nepheline syenites showing assemblage of nepheline, biotite, K-feldspar and minor quartz
d) Oscillatory zoning and secondary alteration i.e serictization
e) Perthite texture developed with myrmekitic intergrowth
f) Biotite (Bio) in association with potassium feldspar (Kfs) and myrmekitic intergrowth

While the nonporphyritic coarse-grain granites consist of quartz, microcline, plagioclase, biotite, amphibole, with various accessory minerals (Fig.3b). The fine-grained nepheline syenite thin section shows a holocrystalline texture dominated by alkali feldspar with interstitial nepheline displaying low relief and weak birefringence. Nepheline commonly shows alteration, and the poor absence of quartz confirms its undersaturated alkaline nature (Fig.3c). The crystallization of plagioclase feldspar with oscillatory zoning reveals a change in composition caused by variations in temperature and other chemical parameters in the melt (Fig.3d). K-feldspar and plagioclase subsolidus dissolve at a delayed cooling rate to

form perthite, one of the primary textures found in Kyrdem granitoids (Fig.3e). One feature that distinguishes Kyrdem granitoids is their myrmekitic texture (Fig.3f), which is characterised by intergrowths of quartz and plagioclase along the K-feldspar borders. This texture formation demonstrates the high levels of hydrothermal fluid activity in the mineral phases that preceded its genesis. The late-stage magmatic processes that produced this texture were the result of fluids supporting metasomatic activity during the last phases of magmatic activity. Petrographic textural evidence with an increase in the proportion of mafic minerals from place to place, supporting magma blending and assimilation, adds to the complexity of the petrography of the KG.

Geochemical Characteristics

As shown in Table 1, the SiO_2 weight percentage, as ranges from 58.9 to 70.8 wt%, characterises the granitoid suite and implies an intermediate to highly felsic composition with moderate to high Al_2O_3 (11.91 to 18.25 wt%), K_2O (4.8 to 11 wt%), moderate Na_2O (2.06 to 3.63 wt%), FeO (2.35-6.91wt%) and low CaO (1.45 to 2.93 wt%), MgO (0.37 to 2 wt%). Except for the one fine-grained granitoid samples, which plot inside the field of nepheline syenite (Fig.4a), all of the analyzed KG samples plot within the granite field in the TAS diagram (following Cox et al., 1979). For fine-grained granitoid to porphyritic to non-porphyritic variety, the SiO_2 vs. K_2O+Na_2O-CaO binary plot (Frost et al., 2001) indicates an alignment within the alkalic to calc-alkalic to alkalic-calcic series (Fig.4b). This is characterised by a relative composition of granitoids that shifts with increased SiO_2 content from alkalic to calc-alkalic to alkali-calcic (Frost et al., 2001) high content of K_2O, Ba, and Sr (Table 1).

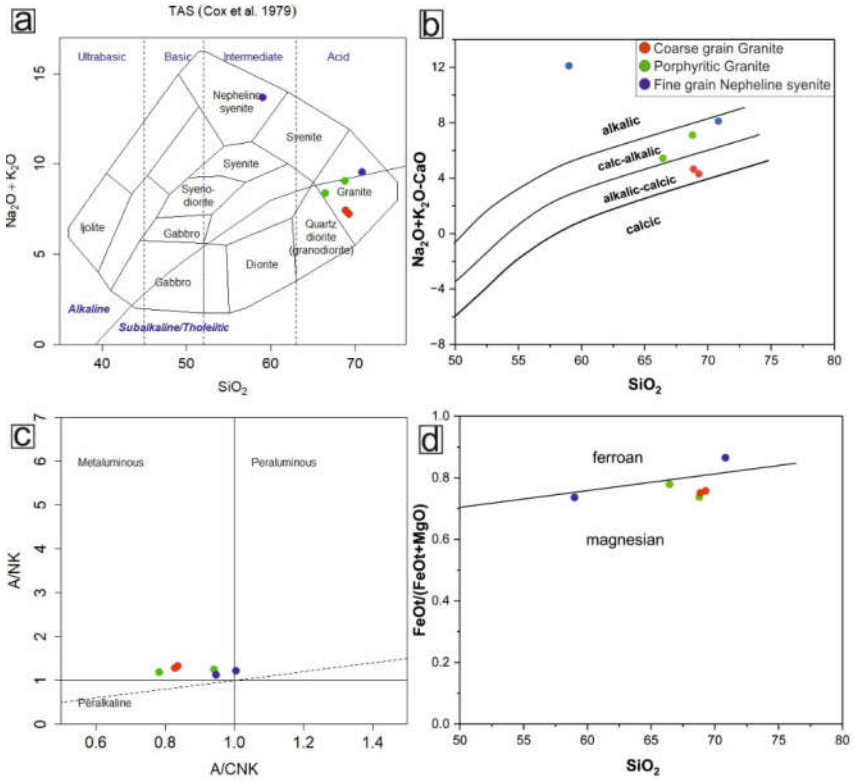

Figure 4: Major element discrimination diagrams for the KG

a) TAS diagram of granite samples (after Cox et al., 1979)

b) SiO_2 vs (Na_2O+K_2O-CaO) Irvine–Baragar diagram (Proposed by Irvine & Baragar (1971)

c) Molar Al_2O_3/(Na_2O+K_2O) versus molar Al_2O_3/($CaO+Na_2O+K_2O$) diagram (after Chappel and White 1992)

d) SiO_2 vs FeO/(FeO + MgO) diagram (after Frost et al., 2001)

Additionally, the majority of the granitoids exhibit metaluminous characteristics, with nepheline syenite displaying peraluminous character (Fig.4c). This indicates an I-type affinity for Kyrdem granitoids (Maniar and Piccoli 1989), with aluminum saturation index (A/CNK ratios) ranging from 0.78 to 1 (Table 1). Furthermore, an acidic magma source is suggested by the modest amounts of MgO (avg. ~1.57 wt%), Fe_2O_3 (avg. 5.03 wt%), and CaO (avg. 2.27 wt%). While one fine-grained nepheline syenite sample exhibits ferroan character, the majority of the KG samples have magnesian character (Table1, Fig.4d). Harker variation diagrams show both linear positive and negative trends in different oxides, which may indicate crystal fractionation or melt contamination (Fig.5). Continual change in the major oxides as SiO_2 increases indicates that fractional crystallization, the primary magmatic differentiation process, governs the chemistry of the rocks. The reverse linear trends for TiO_2, Fe_2O_3, MgO, and CaO indicate that Fe-Mg-Ca-rich minerals, such as olivine, pyroxenes, and amphiboles, were first taken from the source magma and then remained there (Fig.5). The residual melt was then converted into a highly differentiated, SiO_2-rich granite composition as a result of this depletion. Plagioclase feldspar has always been present during crystallisation, as evidenced by the comparatively constant proportion of Al_2O_3 in the SiO_2 range. However, as differentiation progresses, the alkali elements in the residual melt gradually increase, as evidenced by the growing positive connection between Na_2O and K_2O. The varied pattern of P_2O_5, which displays an increase followed by a drop, can be explained by apatite accession during the latter phases of crystallisation. The residual magma continues to accumulate with elements that are mostly found in minerals that develop late and at low temperatures (K, Na, and Si) after the initial minerals that crystallise at high temperatures (Fe, Mg, Ca, and Ti) have been removed.

Table. 1 Whole rock major oxides (wt. %), trace and REE (in ppm) composition of southern Kyrdem Granitoids, Shilong Plateau, Meghalaya.

	Porphyry Granite		Coarse Grain		Fine Grain	
Major oxides	**NO LIZA 1**	**JU LIZA 1**	**NON LIZA 1**	**UQ LIZA 1**	**MK LIZA 1**	**UQ LIZA 3F**
SiO_2	68.77	66.44	69.27	68.86	70.82	58.99
TiO_2	0.46	0.76	0.57	0.60	0.21	0.70
Al_2O_3	13.67	12.22	12.18	11.91	15.12	18.25
FeO*	4.32	6.91	5.64	6.03	2.35	4.90
MnO	0.05	0.08	0.07	0.07	0.04	0.05
MgO	1.53	1.96	1.80	2.00	0.37	1.76
CaO	1.96	2.92	2.93	2.79	1.45	1.59
Na_2O	2.06	2.23	2.43	2.21	3.63	2.71
K_2O	7.00	6.14	4.82	5.23	5.94	11.00
P_2O_5	0.18	0.34	0.28	0.30	0.08	0.04
Total	100	100	100	100	100	100
Ratio						
K_2O/Na_2O	3.40	2.76	1.99	2.36	1.63	4.06
K_2O/Al_2O_3	0.51	0.50	0.40	0.44	0.39	0.60
Na_2O/Al_2O_3	0.15	0.18	0.20	0.19	0.24	0.15
FeO*/(FeO*+MgO)	0.74	0.78	0.76	0.75	0.86	0.74
A/CNK	0.94	0.78	0.84	0.83	1.00	0.95
A/NK	1.25	1.19	1.32	1.28	1.22	1.12

Na_2O+K_2O	8.93	8.31	7.18	7.39	9.44	13.57
Trace Element (ppm)						
Li	25.21	49.44	39.12	33.33	33.56	23.58
Sc	10.73	9.79	13.36	10.22	5.80	2.88
V	57.54	98.43	87.25	84.94	15.40	80.22
Cr	11.36	14.96	16.16	15.15	12.37	25.22
Co	6.50	11.17	9.95	9.07	2.46	8.45
Ni	4.14	5.17	5.27	9.99	5.56	4.72
Cu	20.99	19.37	13.46	22.62	25.65	26.09
Zn	46.53	38.62	72.17	39.64	48.93	29.99
Ga	18.70	21.76	25.07	21.11	28.13	22.88
Rb	263.46	264.42	275.11	230.75	443.69	296.62
Sr	533.81	586.84	516.08	494.11	103.10	410.87
Y	92.48	70.82	66.65	57.56	59.41	6.96
Zr	642.74	848.34	1111.37	876.65	408.16	501.17
Nb	26.68	30.05	32.30	26.80	33.37	19.36
Cs	5.61	4.89	6.40	4.06	10.15	1.95
Ba	2703.87	2196.14	1439.20	1508.49	709.71	3007.51
La	98.38	109.60	181.72	121.95	137.44	30.50
Ce	212.04	242.10	366.60	255.52	278.69	59.44
Pr	25.33	29.96	39.40	29.24	30.22	6.00
Nd	92.39	111.56	130.91	101.54	99.91	19.12
Sm	18.06	20.93	20.60	17.01	18.19	3.81
Eu	3.34	3.32	3.08	2.76	1.49	0.85
Gd	15.38	15.88	15.04	12.76	13.04	1.89
Tb	2.57	2.46	2.29	1.95	2.03	0.27
Dy	15.72	13.59	12.38	10.64	11.25	1.37
Ho	3.13	2.56	2.33	2.00	2.11	0.27
Er	8.48	6.69	6.32	5.37	5.55	0.75
Tm	1.21	0.98	0.94	0.80	0.81	0.13
Yb	7.71	6.41	6.31	5.36	5.30	0.95
Lu	1.00	0.88	0.90	0.75	0.82	0.16
Hf	12.47	20.76	24.05	20.54	12.22	13.81
Ta	2.52	2.08	2.42	2.03	2.05	0.93
Pb	64.65	55.58	52.52	47.17	88.07	75.14
Th	38.70	45.82	86.48	55.83	128.03	16.30
U	5.41	6.96	10.03	7.97	29.30	2.18
∑REE	504.70	566.90	788.81	567.66	606.84	125.50
Ratio						
Ba/Th	69.87	47.93	16.64	27.02	5.54	184.50
Ba/La	27.48	20.04	7.92	12.37	5.16	98.62
Ti/Zr	4.20	5.26	3.01	4.03	2.96	8.17
Th/Yb	5.02	7.15	13.70	10.42	24.13	17.19

U/Th	0.14	0.15	0.12	0.14	0.23	0.13
Rb/Sr	0.49	0.45	0.53	0.47	4.30	0.72
Nb/Y	0.29	0.42	0.48	0.47	0.56	2.78
Nb/Yb	3.46	4.69	5.12	5.00	6.29	20.42
Nb/Ta	10.58	14.43	13.36	13.20	16.28	20.77
Zr/Y	6.95	11.98	16.67	15.23	6.87	72.06
Zr/Yb	83.34	132.39	176.01	163.68	76.94	528.39
Zr/Hf	51.54	40.86	46.21	42.69	33.41	36.29
10000*Ga/Al	2.62	3.39	3.93	3.37	3.57	2.39
Mg#	21.63	18.06	19.90	20.49	10.82	21.75
Nb+Y	119.16	100.87	98.96	84.37	92.78	26.32
Yb+Ta	10.23	8.49	8.73	7.39	7.35	1.88
∑REE+Zr+Y	1239.97	1486.06	1966.83	1501.87	1074.41	633.63
Zr+Nb+Ce+Y	973.94	1191.31	1576.93	1216.55	779.63	586.92

In terms of trace element characteristics, Large ion lithophile elements (LILE) (avg. (Rb+Sr+Ba)~2663 ppm), Ba values vary greatly, ranging from 709-3000 ppm, Sr (103-586 ppm) and Rb levels range between 230.7 and 443.6 ppm, with total REE abundance of Kyrdem granites is (avg.~526 ppm) (Table 1). The Ni contents within these granitoids range from 4.1 to 10 ppm. Additionally, the enrichment of high field strength elements (average-Zr~731 ppm, U~10.3 ppm, Th~61.8 ppm, Y~58.98 ppm, and Ga~22.9 ppm) in the majority of the KG indicates that the magma was highly evolved (Table 1). The spike in zirconium (Zr) indicates that the melt has attained zircon saturation and begun to crystallize. Because sediment-derived melts and continental crust are naturally concentrated in these elements, high Th–U can also indicate a major crustal contribution. An A-type or within-plate affinity for the granite is further suggested when this enrichment coexists with significant Zr, Nb, Y, and REE. The trace element geochemical variation diagrams for Kyrdem granitoids reveal distinct patterns of trace elements with increasing SiO_2 content (Fig. 6). This suggests that there are significant factors in magma differentiation. The general decreasing trends of vanadium (V), yttrium (Y), niobium (Nb), and scandium (Sc) show a progressive decline of these elements with increasing silica contents, a phenomenon associated with element depletion through fractional crystallization by the early-forming mafic minerals from the melt (Fig.6). Removal of V and Sc-enriched mafic minerals, as well as accessory phases containing Nb and Y, was most likely significant enough to generate the observed trends. The systematic depletion of trace elements highlights the importance of magmatic differentiation in the formation of Kyrdem granitoids. This movement from less to more developed magma compositions is characterised by increasing SiO_2 content. An enriched fractionated LREE with nearly flat HREE and a strong negative Eu anomaly (Eu/Eu* = 0.19– 0.61) and $(La/Lu)_N$=10.60-26.53) is inferred from the KG coarse porphyritic and non-porphyritic granite and fine-grain nepheline syenite chondrite normalized (Nakamura, 1974) REE patterns (Fig. 7a). This suggests the evolved nature of the melt from a crustal or enriched mantle source with primary plagioclase removal occurred during the granite's fractionation process or it was retained in the residue phase after the source's partial melting. The depletion of HREE points to residual garnet or amphibole in the source, hinting at melting at moderate depths. On the primitive mantle (PM) normalised multi-element variation diagram (in accordance with Sun and McDonough 1989), all of the granitoids under investigation had fractioned and enriched patterns. High-field strength elements (HFSE) up to 1000 times PM and LILEs enriched up to 10-1000 times PM (Fig. 7b), which is strikingly similar to Nongpoh Granitoids.

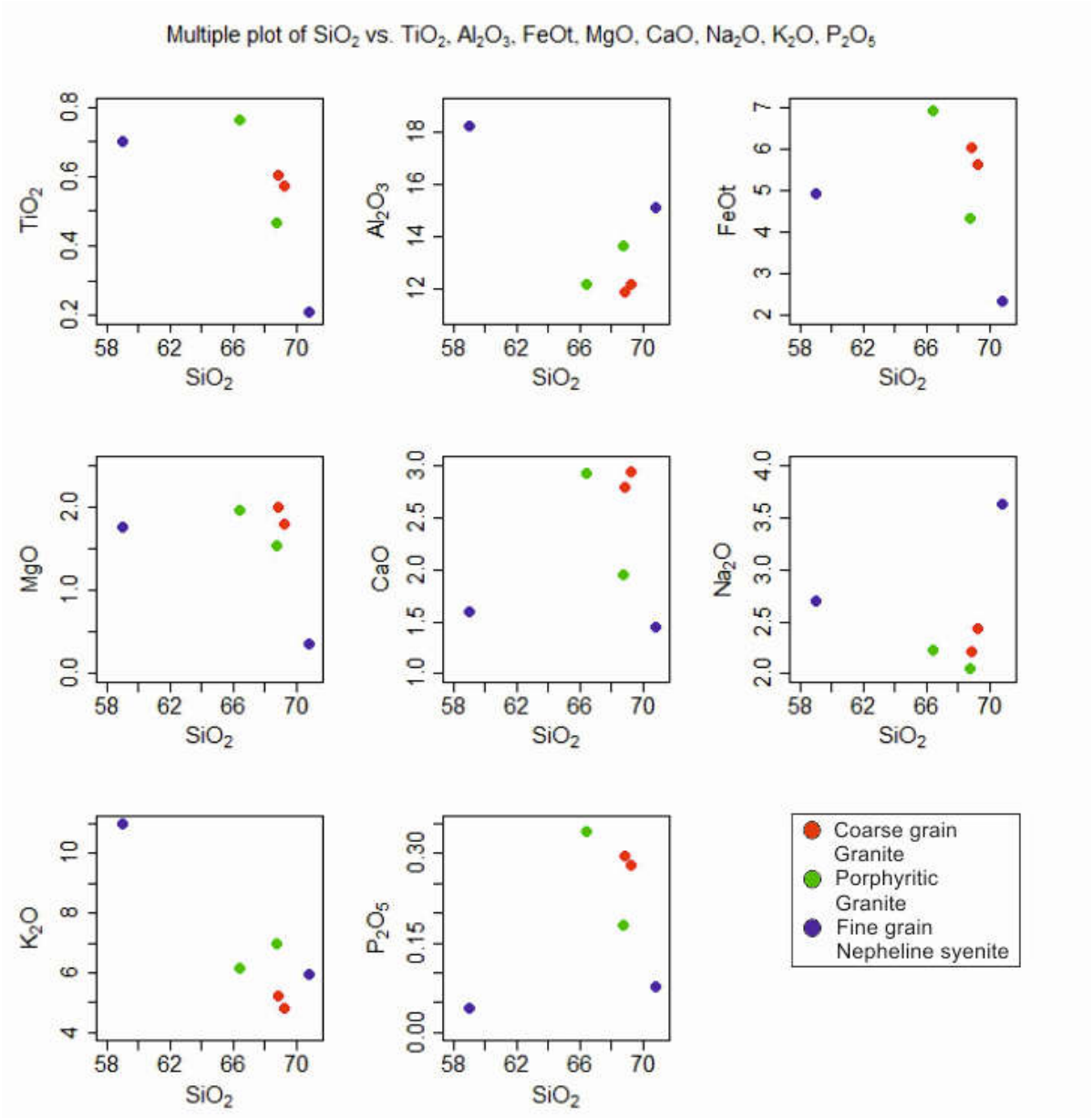

Figure 5: Major oxides vs SiO_2 Harker variation diagrams for K G

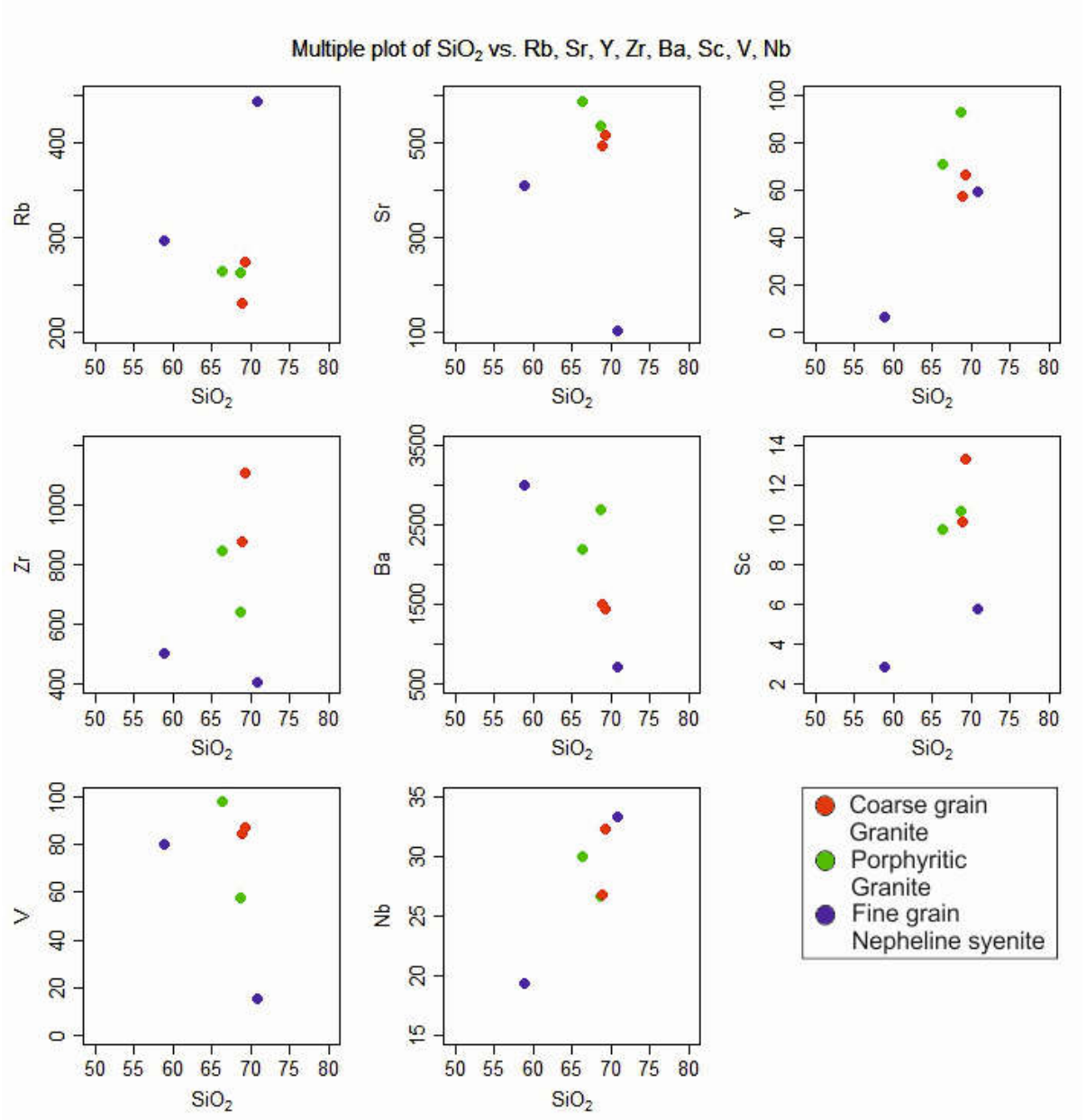

Figure 6: Trace elements vs SiO_2 Harker variation diagrams for K G

The AFM diagram (Irvine and Baragar, 1971) indicates that the Kyrdem granitoids are in the calc-alkaline series (Fig. 8a), which is typical of magmas are formed in subduction zones. It means that water-derived magma was inescapable in the granitoids, and so iron did not cool to a high concentration level. The existence of minerals such as amphibole and biotite indicated that these rocks had gone through fractional crystallisation during the magmatic cycle, resulting in a melt devoid of iron. This water-mediated iron depletion mechanism is one of the mechanisms that has long been identified in subduction zones. The southern KG hence point to a subduction-related origin, with oxidation and crystallization playing an important role in magma formation. These felsic melt, as evidenced by their presence in the granite to nepheline syenite field, and their alkalic to alkalic-calcic composition, suggests that the Kyrdem granitoids formed in a tectonic setting where subduction processes influence

magma formation. Differentiation was evident in the magmas with low silica content (SiO_2) and high total alkalis (Na_2O+K_2O) that were produced by fractional crystallization and crustal assimilation. The metaluminous behaviour to moderately peraluminous, indicating a significant increase in aluminum saturation suggests that fractional crystallization and a little amount of crustal material assimilation followed the formation of an I-type magma with minimal crustal participation. There is a noticeable negative Ti anomaly in the plot (Fig. 7b), showing the strong enrichment in LILE elements such as Rb, Ba, and Th, combined with the depletion of HFSE like Nb, Ta, and Ti, reflects a subduction-related environment as a result of their retention in refractory phases within the subducting slab, and the mobilization of LILEs by fluids originating from the slab are characteristics of subduction zone magmatism. In particular, the negative Ti anomaly indicates that Ti-bearing minerals such as ilmenite were eliminated during fractional crystallisation. The Pb concentration seen in the plot (Fig. 7b) is another feature of subduction zone magmatism since slab-derived fluids readily mobilise Pb. These trace element patterns demonstrate the intricate interactions between mantle, crust, and slab-derived processes during the development of the Kyrdem granitoids and validate their subduction-related origin.

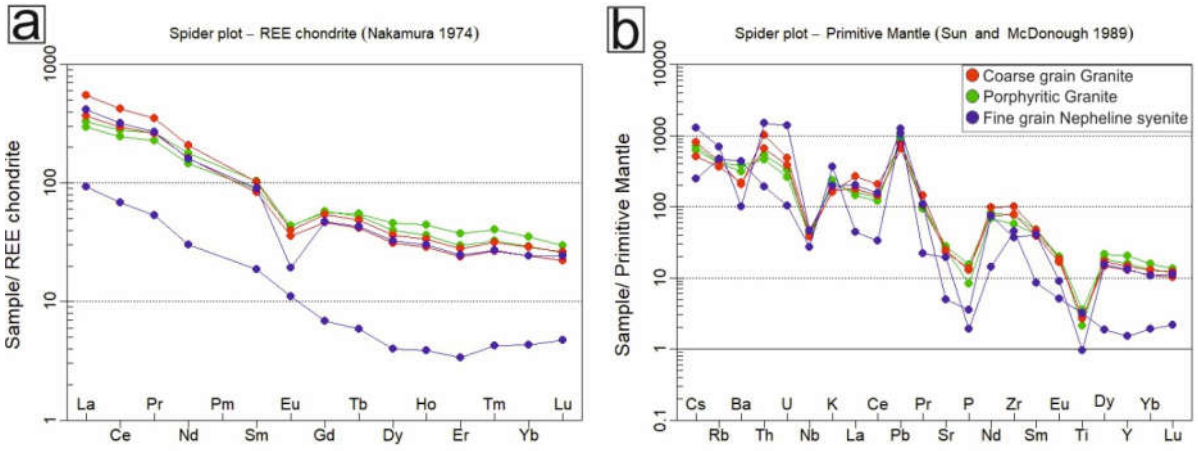

Figure 7:
a) Chondrite normalised Rare Earth Elements (REE) pattern diagram (normalised values after Nakamura, 1974)
b) PM normalised Multi elements spider plot of Kyrdem granitoids (normalised values after Sun & McDonough, 1989)

The R_1–R_2 diagram (Batchelor & Bowden, 1985) (Fig.8b) shows that most of the samples are in the syn-collision field, but some are even near the late-orogenic tectonic realm. This demonstrates that the granite originates from crustal anatexis linked to continental collision, which is followed by either uplift or relaxation. The Y vs Nb, Rb vs (Ta + Yb), Rb vs (Y + Nb) and Yb vs Ta diagrams (Fig. 9) indicate that KG samples plot in the within-plate granite (WPG) field and fine-grained nepheline syenite are plotted nearly to the border of the syn-collisional granite (syn-COLG) field (field after Pearce et al., 1984).

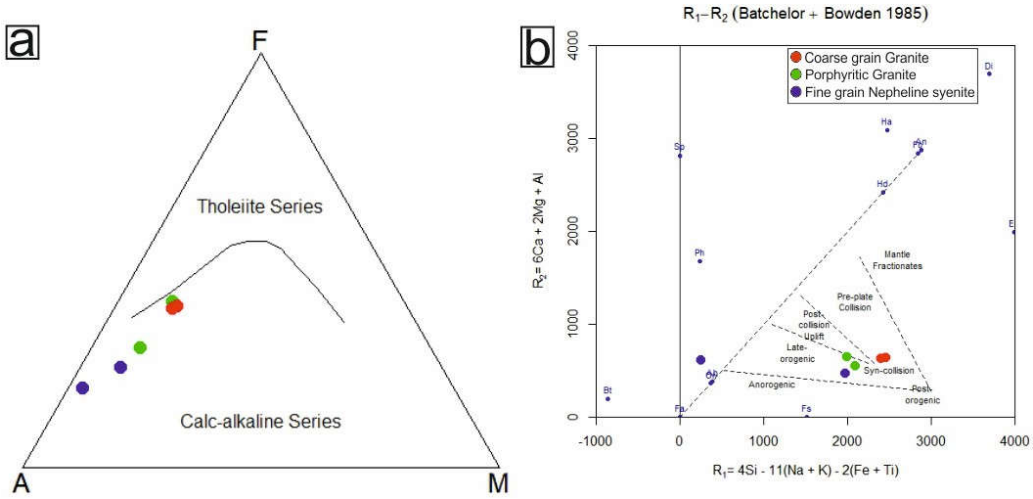

Figure 8:
a) AFM plot (after Irvine and Baragar 1971) showing calc-alkaline trend for KG
b) R_1 versus R_2 tectonic discrimination plot for KG (after Batchelor and Bowden, 1985)

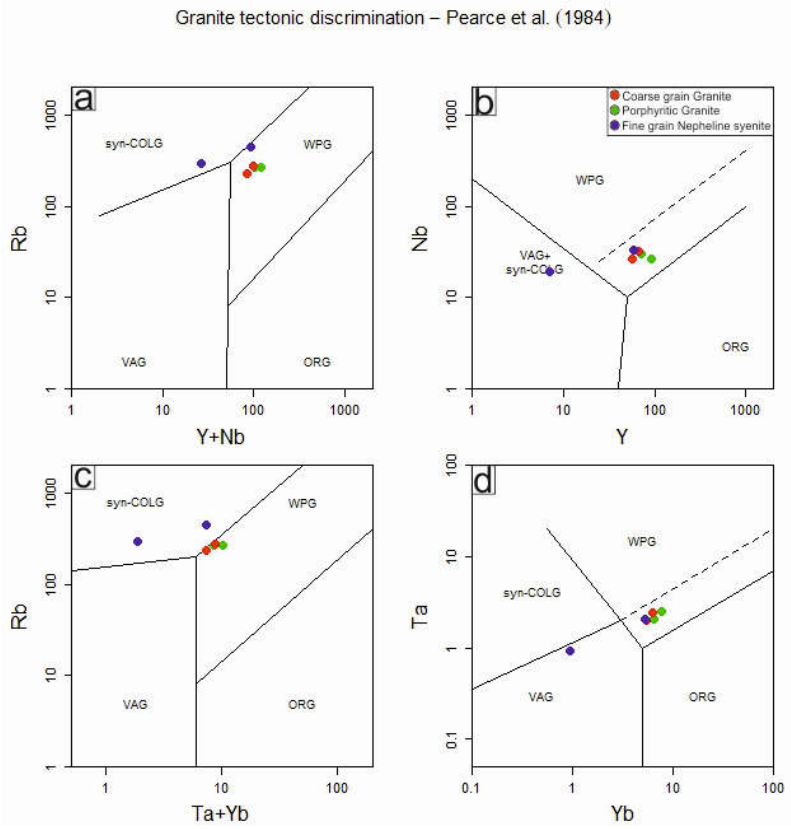

Figure 9: Tectonic discrimination diagram for KG samples fall in the WPG, syn-COLG and VAG field (ORG = Oceanic Ridge Granite; VAG = volcanic arc granitoids; WPG = within plate granites; Syn-COLG = Syn-collisional granites) (after Pearce et al, 1984)
a) Rb vs (Y+Nb) binary plot
b) Y vs Nb binary plot
c) Rb vs (Ta + Yb) binary plot
d) Ta vs Yb diagrams

This geochemical affinity environment indicates that the magmas were generated through interaction between mantle-derived melts and a moderately evolved crustal component during the waning stages of orogeny, followed by the onset of post-collision extension within a within-plate magmatic regime. Overall, the Kyrdem granitoid geochemistry suggests emplacement during a late-collisional to early post-collisional stage, preserving signatures of the final thermal and tectonic pulses of the orogenic event. Similar fine-grained nepheline syenites associated with late-orogenic granitoids are characteristic of post-collisional Pan-African alkaline magmatism, well documented in the Arabian–Nubian Shield (Hassan & Hashad, 1990; Goodenough et al., 2007), Sudan–Egypt ring complexes (Hutchison, 1974), Nigerian Younger Granite Province (Bowden & Kinnaird, 1984), Madagascar (Kröner et al., 2000) and from the Indian Craton too (Rao et al., 2013). These plutonic bodies are silica-undersaturated, mantle-derived melts that formed following crustal thickening and late-orogenic granite intrusion (Black & Liois, 1993).

CONCLUSION

According to a petrological and geochemical analysis of the Kyrdem granitoids rocks are metaluminous, high-Ba–Sr, fractionated I-type granite, characterized by high SiO_2, moderate Al_2O_3 (avg.~13.89 wt%), high Na_2O+K_2O (avg.~9.23 wt%), and elevated Ga/Al (10000×Ga/Al = 3.21). Strong fractional crystallisation and high-temperature melt development are indicated by trace element data showing high Ba (avg.~1927 ppm), Sr (avg.~440 ppm) and high Zr (408-1111 ppm) with moderate Rb (avg.~295 ppm), as well as ∑REE (avg.~526 ppm). Emplacement during post-collisional extension is suggested by its alkaline to alkali-calcic and magnesian character, WPG/post-collision tectonic affinity, and one syn-collision sample. The interaction between mantle-derived melts and a weakly evolved crustal component produced the magma, according to the geochemical signatures, especially the combination of high Ba, Sr, Zr, REE, and moderate Rb. Mantle input provided high-temperature, Ba–Sr–Zr–REE-enriched melt, while crustal assimilation imparted the metaluminous character. A highly fractionated I-type granite generated by crust-mantle hybridization, typical of post-collisional high-Ba-Sr granites, is confirmed by the low ASI (~0.89) and trace element patterns, which clearly rule out a traditional S-type source. This work provides insights into similar geological conditions worldwide during Pan African orogeny and advances our understanding of granitoid genesis in tectonically active and subduction-related regions during Post-Archean time.

ACKNOWLEDGEMENT

We are grateful to the Department of Geology, Mizoram University, CSIR-NGRI, Hyderabad, for providing the laboratory facility needed to complete this work. As well as to Mizoram University for extending administrative facilities. This work is included in Liza Gogoi's doctoral thesis. The authors express gratitude to the editor and reviewers for their insightful feedback.

REFERENCES

Batchelor, R. A., & Bowden, P. (1985). Petrogenetic interpretation of granitoid rock series using multicationic parameters. Chemical Geology, 48(1–4), 43–55. https://doi.org/10.1016/0009-2541(85)90034-8

Black, R., & Liégeois, J.-P. (1993). Cratons, mobile belts, alkaline rocks and continental lithospheric mantle: The Pan-African testimony. Journal of the Geological Society, 150(1), 89–98. https://doi.org/10.1144/gsjgs.150.1.0088

Bowden, P., & Kinnaird, J. A. (1984). Geological, geochemical and mineralogical aspects of the Younger Granite Province of Nigeria. Journal of African Earth Sciences, 2(1), 47–64.

Chappell, B. W., & White, A. J. R. (1992). I- and S-type granites in the Lachlan Fold Belt. Earth and Environmental Science Transactions of the Royal Society of Edinburgh, 83(1–2), 1–26. https://doi.org/10.1017/S0263593300007720

Chatterjee, N. (2017). Constraints from monazite and xenotime growth modelling in the Mn CKFMASH-PYC e system on the P–T path of a metapelite from Shillong-Meghalaya Plateau: Implications for the Indian shield assembly. Journal of Metamorphic Geology, 35(4), 393–412. https://doi.org/10.1111/jmg.12237

Choudhury, D. K., Pradhan, A. K., Zakaulla, S., & Umamaheswar, K. (2012). Geochemistry and petrogenesis of anorogenic (?) Granitoids of West Garo Hills, Meghalaya. Journal of the Geological Society of India, 80(2), 276–286. https://doi.org/10.1007/s12594-012-0138-4

Cox, K. G., Bell, J. D., & Pankhurst, R. J. (1979). The interpretation of igneous rocks. George Allen & Unwin. https://doi.org/10.1007/978-94-017-3373-1

Cox, K. G. (Ed.). (2013). The interpretation of igneous rocks. Springer Science+Business Media. https://scispace.com/pdf/the-interpretation-of-igneous-rocks-2gy5juokz8.pdf

Evans, P. (1964). The tectonic framework of Assam. Journal Geological Society of India, 5(1), 80–96. https://doi.org/10.17491/jgsi/1964/050111

Fowler, M. B., Henney, P. J., Darbyshire, D. P. F., & Greenwood, P. B. (2001). Petrogenesis of high Ba–Sr granites: The Rogart pluton, Sutherland. Journal of the Geological Society, 158(3), 521–534. https://doi.org/10.1144/jgs.158.3.521

Frost, B. R., Barnes, C. G., Collins, W. J., Arculus, R. J., Ellis, D. J., & Frost, C. D. (2001). A geochemical classification for granitic rocks. Journal of Petrology, 42(11), 2033–2048. https://doi.org/10.1093/petrology/42.11.2033

Frost, B. R., & Frost, C. D. (2011). Treatise on geochemistry: Essentials of igneous and metamorphic petrology. Elsevier.

Ghatak, A., & Basu, A. R. (2013). Isotopic and trace element geochemistry of alkalic–mafic–ultramafic–carbonatitic complexes and flood basalts in NE India: Origin in a heterogeneous Kerguelen plume. Geochimica et Cosmochimica Acta, 115, 46–72. https://doi.org/10.1016/j.gca.2013.04.004

Ghosh, S., Chakraborty, S., Bhalla, J. K., Paul, D. K., Sarkari, A., Bishui, P. K., & Gupta, S. N. (1991). Geochronology and geochemistry of granite plutons from East Khasi Hills, Meghalaya. Journal Geological Society of India, 37(4), 331–342. https://doi.org/10.17491/jgsi/1991/370403

Ghosh, S., Fallick, A. E., Paul, D. K., & Potts, P. J. (2005). Geochemistry and origin of neoproterozoic granitoids of Meghalaya, northeast India: Implications for linkage with amalgamation of Gondwana supercontinent. Gondwana Research, 8(3), 421–432. https://doi.org/10.1016/S1342-937X(05)71144-8

Ghosh, S., Paul, D. K., Bhalla, J. K., Bishui, P. K., Gupta, S. N., & Chakraborty, S. (1994). New Rb-Sr isotopic ages and geochemistry of granitoids from Meghalaya and their significance in middle-to Late Proterozoic crustal evolution. Indian Minerals, 48.

Goodenough, K. M. et al. (2007). Post-collisional alkaline magmatism in the Arabian–Nubian Shield. Lithos, 97(3–4), 408–426.

Hassan, M. A., & Hashad, A. H. (1990). Granitoids of the Arabian–Nubian shield. Journal of African Earth Sciences, 11(3/4), 315–327.

Hussain, M. F., & Choudhury, D. (2023). Occurrences of high-K calc-alkaline shoshonitic granitoids in the Northeastern part of Shillong Plateau, Meghalaya, India, 125(6). Current Science (00113891).

Hutchison, R. (1974). Geology of the Red Sea Scroll: Alkaline complexes and PanAfrican tectonics. Philosophical Transactions of the Royal Society of London Series. Part A.

Irvine, T. N., & Baragar, W. R. A. F. (1971). A guide to the chemical classification of the common volcanic rocks. Canadian

Journal of Earth Sciences, 8(5), 523–548. https://doi.org/10.1139/e71-055

Kröner, A. et al. (2000). Pan-African magmatism in Madagascar. Precambrian Research, 102, 99–128.

Kuno, H. (1968). Petrology of the alkaline volcanic rocks. Kodansha Limited.

Majumdar, D., & Dutta, P. (2016). Geodynamic evolution of a Pan-African granitoid of extended Dizo Valley in Karbi Hills, NE India: Evidence from geochemistry and isotope geology. Journal of Asian Earth Sciences, 117, 256–268.

Maniar, P. D., & Piccoli, P. M. (1989). Tectonic discrimination of granitoids. Geological Society of America Bulletin, 101(5), 635–643. https://doi.org/10.1130/00167606(1989)101<0635:TDOG>2.3.CO;2

Mazumdar, S. K. (1976). A summary of the Precambrian geology of the Khasi Hills, Meghalaya. Geological Survey of India, Miscellaneous Publication, 23(2), 311–334.

Mazumdar, S. K. (1986). The Precambrian framework of part of the Khasi Hills, Meghalaya. Records of the Geological Survey of India, 117(2).

Nakamura, N. (1974). Determination of REE, Ba, Fe, Mg, Na and K in carbonaceous and ordinary chondrites. Geochimica et Cosmochimica Acta, 38(5), 757–775. https://doi.org/10.1016/0016-7037(74)90149-5

Nandy, D. R. (1980). Tectonic patterns in northeastern India. Indian J. Earth Sci., 7, 103–107.

Pearce, J. A., Harris, N. B. W., & Tindle, A. G. (1984). Trace element discrimination diagrams for the tectonic interpretation of granitic rocks. Journal of Petrology, 25(4), 956–983. https://doi.org/10.1093/petrology/25.4.956

Rao, Y. V. et al. (2013). Geochemistry of the Chimakurti and Kondapalli alkaline complexes: Evidence for Pan-African alkaline magmatism in SE India. Journal of Asian Earth Sciences, 62, 121–136.

Ray, J. S., Pattanayak, S. K., & Pande, K. (2005). Rapid emplacement of the plume–related Sylhet Traps, eastern India: Evidence from 40Ar-39Ar geochronology. Geophysical Research Letters, 32(10). https://doi.org/10.1029/2005GL022586

Rudnick, R. L., & Gao, S. (2003). 3.01—Composition of the continental crust A2—Holland, Heinrich D. In Treatise on geochemistry (pp. 1–64). Elsevier. https://doi.org/10.1016/B0-08-043751-6/03016-4

Saha, A., Ganguly, S., Ray, J., & Chaterjee, N. (2010). Evaluation of phase chemistry and petrochemical aspects of Samchampi-Samteran differentiated alkaline complex of Mikir Hills, northeastern India. Journal of Earth System Science, 119(5), 675–699. https://doi.org/10.1007/s12040-010-0052-3

Satyanarayanan, M., Balaram, V., Sawant, S. S., Subramanyam, K. S. V., Vamsi Krishna,. V., Dasaram, B., & Manikyamba, C. (2018). Rapid determination of REEs, PGEs, and other trace elements in geological and environmental materials by high resolution inductively coupled plasma mass spectrometry. Atomic Spectroscopy, 39(1), 1–15. https://doi.org/10.46770/AS.2018.01.001

Shand, S. J. (1943). The eruptive rocks (2nd ed.). John Wiley & Sons.

Sun, S.-S., & McDonough, W. F. (1989). Chemical and isotopic systematics of oceanic basalts: Implications for mantle composition and processes. In Geological Society (London) Special Publication A. D. Saunders & M. J. Norry (Eds.), Magmatism in the ocean basins, 42(1), 313–345. https://doi.org/10.1144/GSL.SP.1989.042.01.19

Yin, A., Dubey, C. S., Webb, A. A. G., Kelty, T. K., Grove, M., Gehrels, G. E., & Burgess, W. P. (2010). Geologic correlation of the Himalayan orogen and Indian craton: Part 1. Journal of structural geology, U-Pb zircon geochronology, and tectonic evolution of the Shillong Plateau and its neighboring regions in NE India [Bulletin], 122(3–4) (pp. 336–359).

Zhang, Z.-Y., Wang, Y.-H., Zhang, F.-F., Liu, J.-J., Zhang, W., & Wen, X.-Y. (2021). Origin of high Ba–Sr granitoids at Chigou in central China and implications for Cu mineralization: Insights from whole-rock geochemistry, zircon U–Pb dating, Lu–Hf isotopes and molybdenite Re-Os systematics. Ore Geology Reviews, 138, Article 104416. https://doi.org/10.1016/j.oregeorev.2021.104416

****